

Bootstrap based uncertainty bands for prediction in functional kriging

MARIA FRANCO-VILLORIA and ROSARIA IGNACCOLO*

Department of Economics and Statistics “Cognetti de Martiis”

University of Torino

Abstract

The increasing interest in spatially correlated functional data has led to the development of appropriate geostatistical techniques. Prediction of a curve at an unmonitored location can be obtained using a functional kriging with external drift model that takes into account the effect of exogenous variables (either scalar or functional). Nevertheless uncertainty evaluation for functional spatial prediction remains an open issue. We propose a semi-parametric bootstrap for spatially correlated functional data that allows to evaluate the uncertainty of a predicted curve. Prediction bands are obtained by ordering the bootstrapped predicted curves in two different ways according to band depth and L^2 distance. The performance of the proposed methodology is assessed via a simulation study. Moreover, the approach is illustrated on a well known data set of Canadian temperature and on a real data set of PM₁₀ concentration in the Piemonte region, Italy. Based on the results it can be concluded that the method is computationally feasible and suitable for quantifying the uncertainty around a predicted curve.

Keywords: Geostatistics; functional data modelling; trace-variogram; generalized additive models; band depth; B-splines

1 Introduction

Kriging is a well known prediction method in the geostatistics community (see e.g. [3]); it allows to predict a (scalar) random field or spatial process $\{Z(s), s \in D \subseteq R^2\}$ in a new spatial location s_0 given a set of observed values $Z = (Z(s_1), \dots, Z(s_n))$, taking into account the underlying correlation structure. Spatially dependent functional data (see e.g. the last two chapters of the book by Horváth and Kokoszka [13]) have received increasing interest over the last few years. Geostatistical techniques for functional data were first introduced in the pioneering work

*Corresponding author. Email: maria.francovilloria@unito.it and rosaria.ignaccolo@unito.it

of Goulard and Voltz (1993) [12], but the development of such techniques is rather recent. The simplest case would be that of ordinary kriging, which allows to predict a curve at an unmonitored site under the assumption of a constant mean (see e.g. [5, 11, 19]). The case of a mean function that depends on longitude and latitude was considered in [1, 18, 23]. In their work, Ignaccolo et al. [15] consider more complex forms of non-stationarity, where the mean function may depend on exogenous variables (either scalar or functional), developing the so called kriging with external drift - or regression kriging - in a functional data setting. While much effort has been put in prediction, the uncertainty of a predicted curve remains an open issue, since there is no functional version of the kriging variance. The lack of a distribution function in the functional framework leads to the use of resampling methods for confidence band calculation. In this context, Cuevas et al. [4] consider the standard bootstrap and a smoothed version of it to obtain confidence intervals for location estimators; an informal discussion on the asymptotic validity of the bootstrap approach in a functional framework can also be found in their paper. Further, Ferraty et al. [6] propose using “wild bootstrapping” in the case of a regression model with scalar response and functional covariate. In their method, the scalar errors (assumed to be independent) are multiplied by random variables (constrained to satisfy certain properties) to obtain a bootstrap sample. When the response variable and hence the errors are both functional, to evaluate uncertainty of a predicted curve (obtained from kriging with external drift), we propose to extend the semi-parametric bootstrap approach for spatially correlated data introduced by Iranpanah et al. [16] to the case of functional data.

The paper is organized as follows. In Section 2, we summarize the kriging with external drift (FKED) methodology developed in [15] and extend it to take into account spatial correlation when estimating the drift coefficients by means of an iterative algorithm. In Section 3 we propose a method for deriving prediction bands in the general FKED setting. A simulation study is presented in Section 4 to evaluate the performance of the proposed method, followed by an application to two real data sets. All computations are coded in R [20]. A discussion completes the paper.

2 Functional kriging with external drift (FKED)

Let $\Upsilon_s = \{Y_s(t); t \in T\}$ be a functional random variable observed at location $s \in D \subseteq \mathbb{R}^d$, whose realization is a function of $t \in T$, where T is a compact subset of \mathbb{R} . Assume that we observe a sample of curves Υ_{s_i} , for $s_i \in D$, $i = 1, \dots, n$, taking values in a separable Hilbert space of square integrable functions. The set $\{\Upsilon_s, s \in D\}$ constitutes a functional random field or a

spatial functional process [5] that is not necessarily stationary. The following model is assumed:

$$\Upsilon_s = \mu_s + \epsilon_s, \quad (1)$$

where μ_s is the drift describing a spatial trend and ϵ_s is a zero-mean, second-order stationary and isotropic residual random field. At a fixed site s_i , $i = 1, \dots, n$, and domain point t , the model can be rewritten as a functional concurrent linear model [15]

$$Y_{s_i}(t) = \mu_{s_i}(t) + \epsilon_{s_i}(t) \quad (2)$$

where $\epsilon_{s_i}(t)$ represents the residual spatial functional process $\{\epsilon_s(t), t \in T, s \in D\}$ at the site s_i . The drift term can be expressed in terms of a set of scalar and functional covariates:

$$\mu_{s_i}(t) = \alpha(t) + \sum_p \gamma_p(t) C_{p,i} + \sum_q \beta_q(t) X_{q,i}(t) \quad (3)$$

where $\alpha(t)$ is a functional intercept, $C_{p,i}$ is the p -th scalar covariate at site s_i , $X_{q,i}$ is the q -th functional covariate at site s_i and $\gamma_p(t)$ and $\beta_q(t)$ are the covariate functional coefficients. Model (3) parameters can be estimated by means of a generalized additive model (GAM) representation using the R package `mgcv` (see [15], [30] and [29] for details).

To take into account the spatial correlation between functional observations when estimating the drift term, we propose an iterative algorithm that considers the term $\epsilon_{s_i}(t)$ as a functional random intercept [25] (i.e. a location specific smooth residual) with a given covariance structure. An iterative algorithm is also proposed in [18] to estimate drift coefficients for scalar covariates in universal kriging, as well as in [14] to take into account the heteroskedasticity of functional residuals. The algorithm can be summarized as follows:

1. Fit a standard functional concurrent linear model; estimate the drift term $\mu_{s_i}(t)$ following (3) assuming independent functional observations and obtain the functional residuals $e_{s_i}(t) = Y_{s_i}(t) - \hat{\mu}_{s_i}(t)$.
2. Estimate the correlation matrix K of the residual spatial functional process using the trace-semivariogram [11]. This is defined, for a zero-mean weakly-stationary process, as $v(h) = \int_T \frac{1}{2} \text{Var}(e_{s_i}(t) - e_{s_j}(t)) dt$ where $h = \|s_i - s_j\|$ represents the Euclidean distance between locations s_i and s_j . The trace-semivariogram can be estimated as:

$$\hat{v}(h) = \frac{1}{2|N(h)|} \sum_{i,j \in N(h)} \int_T (\epsilon_{s_i}(t) - \epsilon_{s_j}(t))^2 dt$$

where $N(h) = \{(s_i, s_j) : \|s_i - s_j\| = h\}$. The estimate becomes computationally efficient

when data are expressed using cubic splines, as integration can be avoided by re-expressing the integral in terms of the spline coefficients and basis [11]. Once estimated, the empirical trace-semivariogram provides a cloud of points $(h_g, \hat{v}(h_g)), g = 1, \dots, G$ to which a parametric model (e.g. exponential, spherical, Matérn) can be fitted as in classical geostatistics.

3. Fit model (2) considering the term $\epsilon_{s_i}(t)$ as a functional random effect, following [25], where the inverse of the estimated correlation matrix \hat{K} is used as the precision matrix for a random field across locations.
4. Obtain the functional residuals $e_{s_i}(t) = Y_{s_i}(t) - \hat{\mu}_{s_i}(t)$. Return to step (2) and iterate.

The generalized additive model representation of model (2) can be re-expressed as a mixed effects model [24, 26] whose parameters are estimated using REML [31]. The algorithm's convergence is determined based on the *AIC*, since the effective degrees of freedom may change from iteration to iteration. Convergence is reached when the *AIC* rate is smaller than 0.1%, where the criterion rate at the j -th iteration is calculated as

$$AICrate = \left| \frac{AIC^j - AIC^{j-1}}{AIC^{j-1}} \right|.$$

The resulting functional residuals (at the last iteration) $e_{s_i}(t) = Y_{s_i}(t) - \hat{\mu}_{s_i}(t)$ can be used to predict the residual curve at an unmonitored site s_0 via one of three kriging options: 1) ordinary kriging for functional data [11], according to which $\hat{e}_{s_0}(t) = \sum_{i=1}^n \lambda_i e_{s_i}(t)$, with kriging coefficients $\lambda_i \in \mathbb{R}$; 2) continuous time-varying kriging [10], where the kriging coefficients $\lambda_i(t)$ now depend on t and 3) functional kriging total model [9, 19], where the kriging coefficients are defined on $T \times T$ and

$$\hat{e}_{s_0}(t) = \sum_{i=1}^n \int_T \lambda_i(\tau, t) e_{s_i}(\tau) d\tau.$$

Prediction at the unmonitored site s_0 is obtained by adding up, as in the classical regression kriging, the two terms, i.e. $\hat{Y}_{s_0}(t) = \hat{\mu}_{s_0}(t) + \hat{e}_{s_0}(t)$, where $\hat{\mu}_{s_0}(t) = \hat{\alpha}(t) + \sum_p \hat{\gamma}_p(t) C_{p,0} + \sum_q \hat{\beta}_q(t) X_{q,0}(t)$ depends on the covariate values $C_{p,0}$ and $X_{q,0}(\cdot)$ at the site s_0 .

From now on we focus on the ordinary kriging case; this not only has been shown to be preferable when applied to a real dataset [15] but contributes to keep a moderate computational complexity in what follows (the two other cases will be considered in the discussion).

Note that, in practice, data are gathered as a finite discrete set of observations $(t_j, y_{ij}), t_j \in T, j = 1, \dots, M, i = 1, \dots, n$. Thus, before fitting Model (2), raw data need to be transformed into functional observations assuming $y_{ij} = Y_{s_i}(t_j) + \delta_{ij}$, where δ_{ij} represents measurement error and $Y_{s_i}(\cdot)$ is a continuous function that corresponds to a realization of the functional random field $\{\Upsilon_s, s \in D\}$ at site s_i . The conversion from discrete data to curves involves smoothing; we use

cubic B-splines and the R package `fda` [22], choosing the number of basis functions and penalty parameter using functional cross-validation [15].

3 Bootstrap uncertainty bands for functional kriging

Following the work by Iranpanah et al. [16], we propose a semi-parametric bootstrap approach for spatially correlated functional data that allows to obtain uncertainty bands for a predicted curve $\hat{Y}_{s_0}(t)$ at an unmonitored site s_0 . The bootstrapping algorithm can be summarized as follows:

1. Estimate the drift μ_s following Model (3) and subtract it from the observed data to obtain the functional residuals $\epsilon_{s_i}(t) = Y_{s_i}(t) - \hat{\mu}_{s_i}(t)$.
2. The residual spatial correlation will determine the covariance matrix Σ , that can be estimated using the trace-semivariogram as detailed in the previous section.

The estimated covariance matrix can be decomposed using Cholesky decomposition as $\hat{\Sigma} = \hat{L}\hat{L}^T$ and the functional residuals transformed so that they become spatially uncorrelated. In matrix-like notation, this corresponds to:

$$\zeta_{n \times M} = (\zeta(s_1), \dots, \zeta(s_n))' = \hat{L}_{n \times n}^{-1} (Y_{n \times M} - \hat{\mu}_{n \times M}).$$

where $\{\zeta_s(t), t \in T, s \in D\}$ is now a functional random field with identity covariance matrix.

3. Generate B bootstrap samples $\zeta^*(s_1), \dots, \zeta^*(s_n)$ from $\zeta(s_1), \dots, \zeta(s_n)$. This is done using the smoothed bootstrap as suggested in Cuevas et al. [4], where the empirical distribution function of $\{\zeta(s_1), \dots, \zeta(s_n)\}$, denoted as F_n , is replaced by a smooth version \hat{F}_n to avoid appearance of repeated measures in the bootstrap samples. In practical terms, this is equivalent to adding some noise to each originally resampled observation, so that a bootstrap sample $\zeta^*(s_1), \dots, \zeta^*(s_n)$ from \hat{F}_n can be obtained as

$$\zeta_{s_i}^*(t_j) = \zeta_{s_i}^0(t_j) + Z_i(t_j), \quad j = 1, \dots, M,$$

where $\zeta^0(s_i)$ is drawn from F_n and $(Z(t_1), \dots, Z(t_M)) \sim MVN(0_M, \kappa \Sigma_\zeta)$, with Σ_ζ being the covariance matrix of $\{\zeta(t)\}$; the latter can be tuned using a smoothing parameter κ that has to be fixed a priori by the user. However, no rule or indication is found in Cuevas et al. [4] as to how to choose this value, other than trial and error; based on their simulation study, the “rule of thumb” would be to increase the value of κ whenever the number of replicates is not enough to construct a reliable confidence band.

4. The final bootstrap sample $Y_{s_1}^*, \dots, Y_{s_B}^*$ is determined using an inverse transform:

$$Y_{s_i}^*(t) = \hat{\mu}_{s_i}(t) + \hat{L}\zeta_{s_i}^*(t).$$

The functional kriging with external drift model is then fitted to each bootstrap sample to obtain B prediction curves at the unmonitored location s_0 . These B curves need to be somehow ordered so that the quantiles of the distribution (that will determine the upper and lower limits of the prediction band) can be identified. However, the idea of ordering curves is not as straightforward as ordering scalar values, and to our knowledge there is no gold standard for doing so. We consider two different ordering techniques available in the literature.

The first one builds on the idea of band depth [17], that can be defined for any set of k curves. In their paper, Lopez-Pintado and Romo [17] suggest using $k=3$, stating that there is no need to increase k as “the band depth induced order is very stable in k ”. Even for $k=2$, the computational cost is considerable when the sample includes a large number of functional curves; to improve computation times, we have adopted the fast algorithm proposed by Sun and Genton [28] with $k=2$. The band in \mathbb{R}^2 delimited by the curves y_{i_1}, y_{i_2} is defined as

$$B(y_{i_1}, y_{i_2}) = \{(t, y(t)) : t \in T, \min_{r=1,2} y_{i_r}(t) \leq y(t) \leq \max_{r=1,2} y_{i_r}(t)\}.$$

The sample band depth (BD) of a curve $y(t)$ in a set of n curves can be calculated as

$$BD_{n,2}(y) = \binom{n}{2}^{-1} \sum_{1 \leq i_1 < i_2 \leq n} I\{G(y) \subseteq B(y_{i_1}, y_{i_2})\}$$

where $G(y)$ is the graph of a curve $y(t)$ defined as the subset of the plane $G(y) = \{(t, y(t)) : t \in I\}$. Potential problems of using $k = 2$ include ties (i.e. more than one curve with the same depth value) and crossing over of the curves delimiting the band (in which case the band “is degenerated in a point and, with probability one, no other curve will be inside this band” [17]). To avoid these problems and still count with the computationally advantage of using $k = 2$, band depth can be modified to take into account whether a portion of the curve is in the band, giving rise to the modified band depth (MBD) [17]), defined as

$$MBD_{n,2}(y) = \binom{n}{2}^{-1} \sum_{1 \leq i_1 < i_2 \leq n} \frac{\lambda(\{t \in T : \min_{r=i_1, i_2} y_r(t) \leq y(t) \leq \max_{r=i_1, i_2} y_r(t)\})}{\lambda(T)}$$

where λ is the Lebesgue measure on T (for further details see [17]).

The second ordering scheme is based on L^2 distance between curves [4]. In this case, the bootstrap-based predicted curves are ordered based on how distant they are from the originally predicted curve, according to the L^2 distance definition:

$$\|x - y\| = \left(\int_T (x(t) - y(t))^2 dt \right)^{1/2} \quad (4)$$

With this scheme, the lower the distance, the more central the curve is.

The lower/upper limits of a 95% prediction band based on band depth are obtained by taking the pointwise (w.r.t. t) minimum/maximum of the 95% deepest curves (i.e. those closest to the center of the distribution) [27]. On the other hand, the 95% prediction band based on L^2 distance (also referred to as “prediction ball”) is made of the 95% curves closest to the original FKED predicted curve [4].

4 Simulation Study

The performance of the bootstrapping method proposed in Section 3 is evaluated here through a simulation study. Our aim is to analyse the impact of the spatial structure of the functional residual random field, by means of the covariance function parameters (scale and range), as well as that of the ordering technique chosen to derive the uncertainty bands when increasing the number of sites.

Data were simulated using cubic B-splines on a spatial irregular grid (n locations) on $D = [0, 2] \times [0, 3]$ and curve domain $T = [0, 1]$. We used a B-spline basis on T with 10 basis functions. The residual functional random field was built as

$$e_s(t) = \sum_{j=1}^{10} \xi_j(s) B_j(t)$$

where $B_j(t)$ is the j -th basis function evaluated at $t \in T$ (i.e. a curve) and the spatially correlated spline coefficients $\{\xi_j(s), s \in D\}$. These were generated for each j in $1, \dots, 10$ using the same exponential covariance function with range and scale parameters $\phi \in (0.1, 0.3, 0.5)$ and $\sigma^2 \in (1, 2, 4)$ respectively, resulting in 9 different scenarios. The drift was obtained as

$$m_s(t) = \alpha(t) + \beta_1(t)lon + \beta_2(t)lat$$

where lon and lat are the spatial coordinates, $\alpha(t)$ is a functional intercept and $\beta_1(t), \beta_2(t)$ are functional coefficients. The functional coefficients $\alpha(t)$, $\beta_1(t)$ and $\beta_2(t)$ can be expressed in terms of the same B-spline basis with scalar spline coefficients (common for all sites) that are drawn

independently from a standard normal distribution. Finally, simulated observations were built as

$$Y_s^{sim}(t) = m_s(t) + e_s(t) + \xi_s(t)$$

where $\xi(t) = \{\xi_{s_1}(t), \dots, \xi_{s_n}(t)\} \sim N_n(0, 0.09)$ is a vector of random errors for each fixed $t \in [0, 1]$; in practice we consider 101 equally spaced points in $[0, 1]$.

For each simulation scenario, we generated functional data at $n = 25, 50$ and 90 nested locations. Additionally data were generated at 10 more sites (always the same for all three sample sizes) used as validation stations. The locations can be seen in Figure 1, while the simulated data can be seen in Figure 2 for $n = 90$ (note that the cases $n = 25$ and $n = 50$ are just subsets of this).

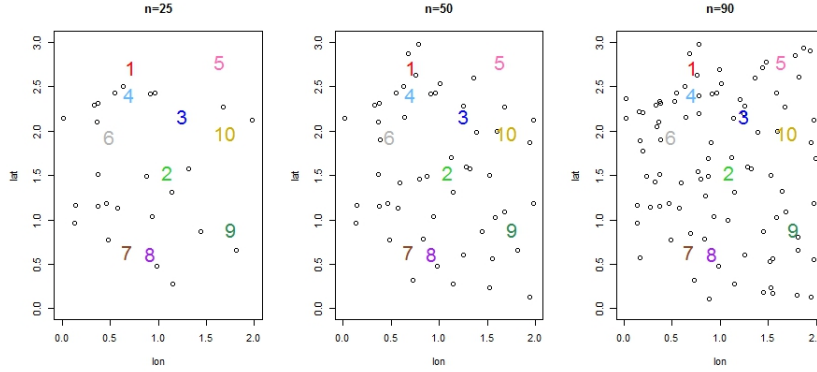


Figure 1: Locations of the 25, 50 and 90 sites used for model fitting. Validation sites numbered 1 to 10.

For each of the three sample sizes, and each simulation scenario, the FKED model presented in Section 2 was applied to the corresponding data set to predict curves at the 10 validation sites. In particular, a drift term depending on longitude and latitude was considered and ordinary kriging was used to obtain the predicted residuals. In practice, the variogram model is chosen automatically among exponential, gaussian and spherical based on minimum SSE. The resulting predicted curves, along with the observed data, can be seen in Figure 3 in the case of $n = 90$ and range and scale parameters $\phi = 0.5$ and $\sigma^2=1$, respectively, for the exponential covariance function in the simulation design. It appears that there is good agreement between simulated and predicted observations. Similar figures for the other cases are available upon request from the authors. Following the algorithm illustrated in Section 3, a bootstrap sample of predicted curves of size $B = 1000$ was obtained for each validation station. We considered two different values for the smoothing parameter κ , 0.01 and 0.05, but there was no evident difference between the resulting uncertainty bands. Since a larger κ leads to adding a larger noise to the original data,

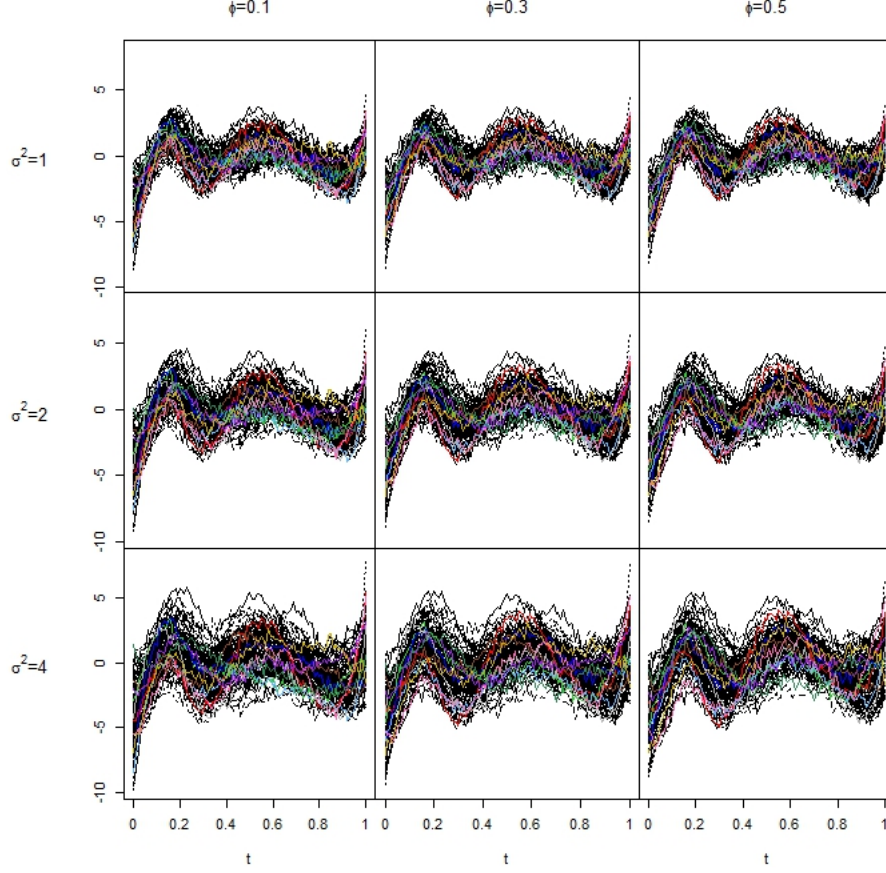


Figure 2: Simulated data ($n=90$) with 10 validation stations curves in color, for each simulation scenario.

the smallest value of $\kappa = 0.01$ was preferred. These 1000 curves were ordered using both distance and band depth, where the latter was calculated using the modified version *MBD*. The resulting 95% prediction balls/bands are shown in Figure 3. Overall, the two uncertainty measures provide very similar prediction bands.

To evaluate the performance of the bootstrap method proposed, we can consider two different indicators: first, the width of the resulting 95% prediction interval, and second, the coverage over the domain T (i.e. the proportion of simulated points within the interval). In Figure 4, we show the band width corresponding to a sample size of $n = 25$ and all simulation scenarios, where the interval has been produced ordering the curves according to band depth, while Figure 5 summarizes the difference in width when using band depth and distance for the same sample size. The remaining figures (for $n = 50, 90$) are not shown here due to space limitations but are available upon request from the authors. As expected, the width of the interval in the curve domain becomes greater towards the borders. As for the effect of the covariance function

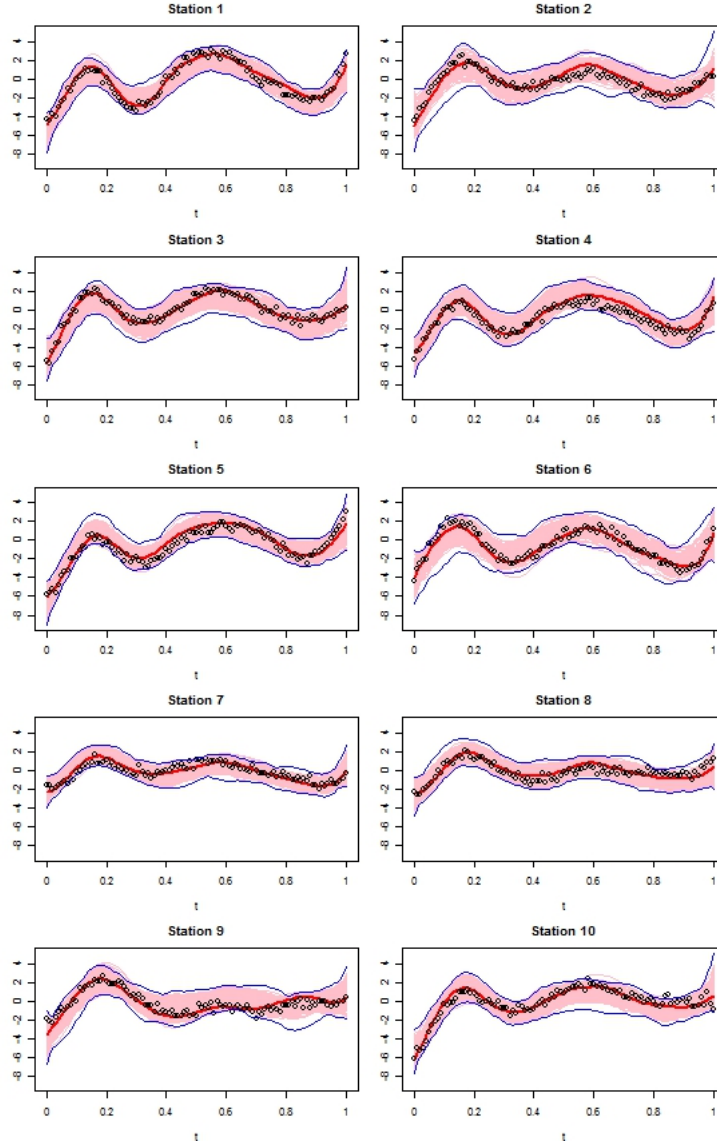


Figure 3: Original data (black dots), FKED predicted curve (solid red line), 95% prediction ball (pink) based on L^2 distance and 95% prediction band (blue) based on MBD for $n=90$, $\sigma^2 = 1$, $\phi = 0.5$.

parameters, greater values of both the range and scale parameters lead to wider prediction bands. The increase in scale parameter (σ^2) leading to an increase in width can be explained by the fact that as σ^2 increases the variability among curves increases too, i.e. the curves become more dissimilar. The increase in width with increasing ϕ is more evident for $\sigma^2 = 4$ than for smaller values of σ^2 . When comparing band depth and distance (Figure 5) it is interesting to see that for $\phi = 0.1$, the depth based interval is practically always wider than the distance based one, regardless of the value of σ^2 . For greater values of ϕ , this systematic difference between the two

ordering techniques is no longer evident. Figure 6 shows the prediction band width, when using band depth for ordering curves, for a fixed simulation scenario ($\sigma^2 = 4$ and $\phi = 0.5$) and all three samples sizes; here it can be seen that as n increases, the width of the interval becomes more stable on T .

On the other hand, the coverage over T is summarized in Figure 7 for all simulation scenarios and sample sizes. This coverage is linked to the width of the interval (the larger the width the larger the coverage) but also to the goodness of FKED prediction because the uncertainty band is built around the predicted curve: if the prediction is far from the original data, the corresponding coverage will be poor, and viceversa. We can see in Figure 7 that when $\phi = 0.1$ for all three sample sizes and all three σ^2 values, the coverage is not so high; this could be due to the fact that in these cases the width of the bands is quite small (as shown in Figure 4 for the case $n = 25$). Instead, when $\phi = 0.03$ or 0.05 , so that there is a moderate to strong spatial correlation, the performance appears good and improves with a large enough sample size.

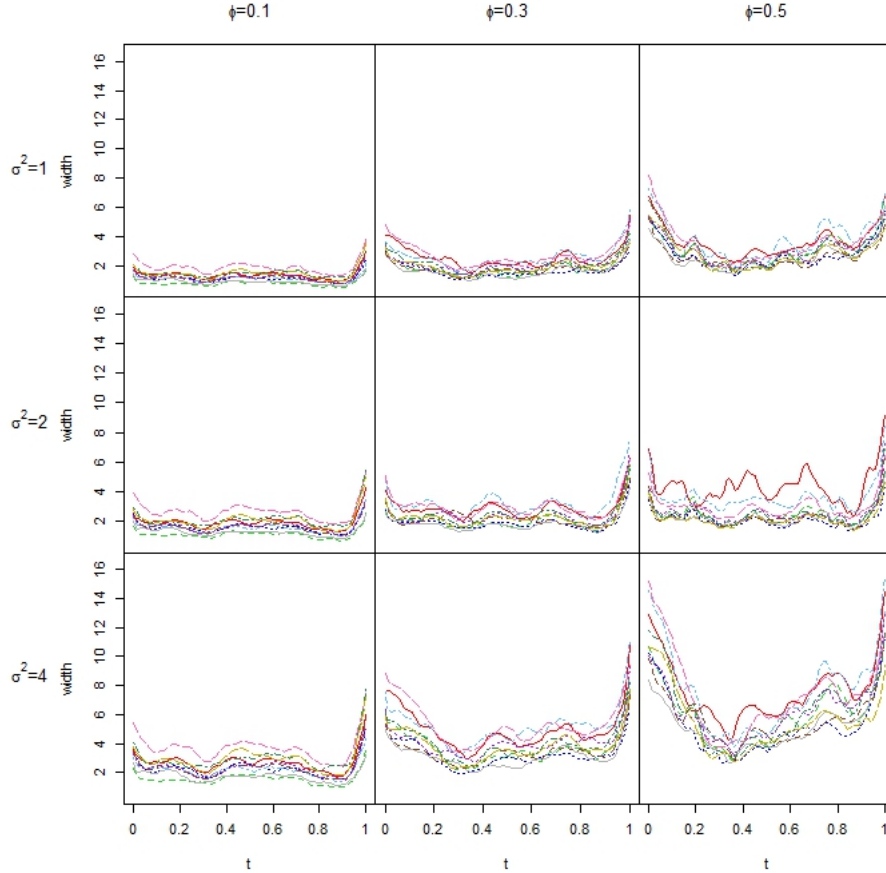


Figure 4: Prediction band width according to band depth ($n = 25$) for 10 validation stations and different simulation scenarios.

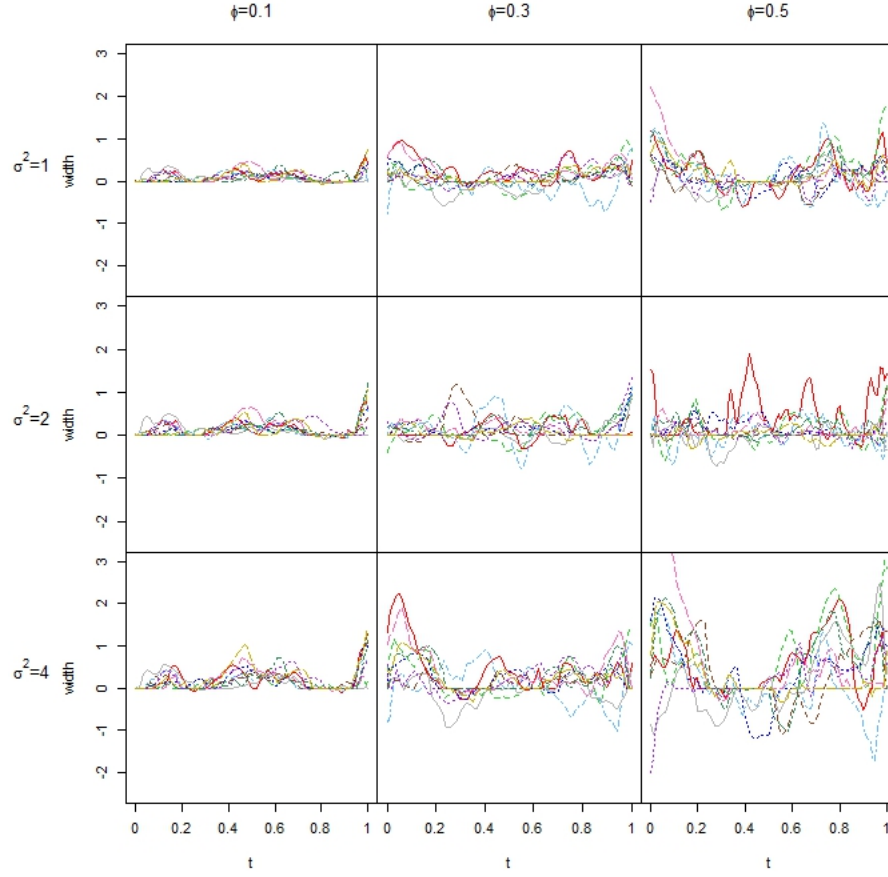


Figure 5: Difference in width (depth-distance) for 10 validation stations and different simulation scenarios when $n = 25$.

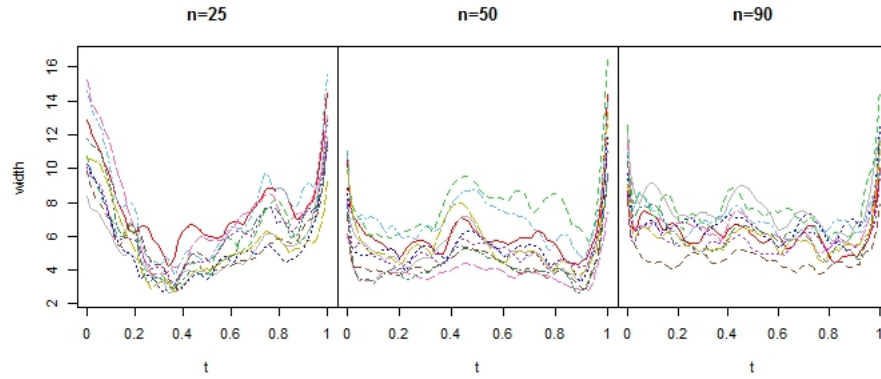


Figure 6: Prediction band width, when using band depth for ordering curves, for a fixed simulation scenario ($\sigma^2 = 4$ and $\phi = 0.5$) and all three samples sizes.

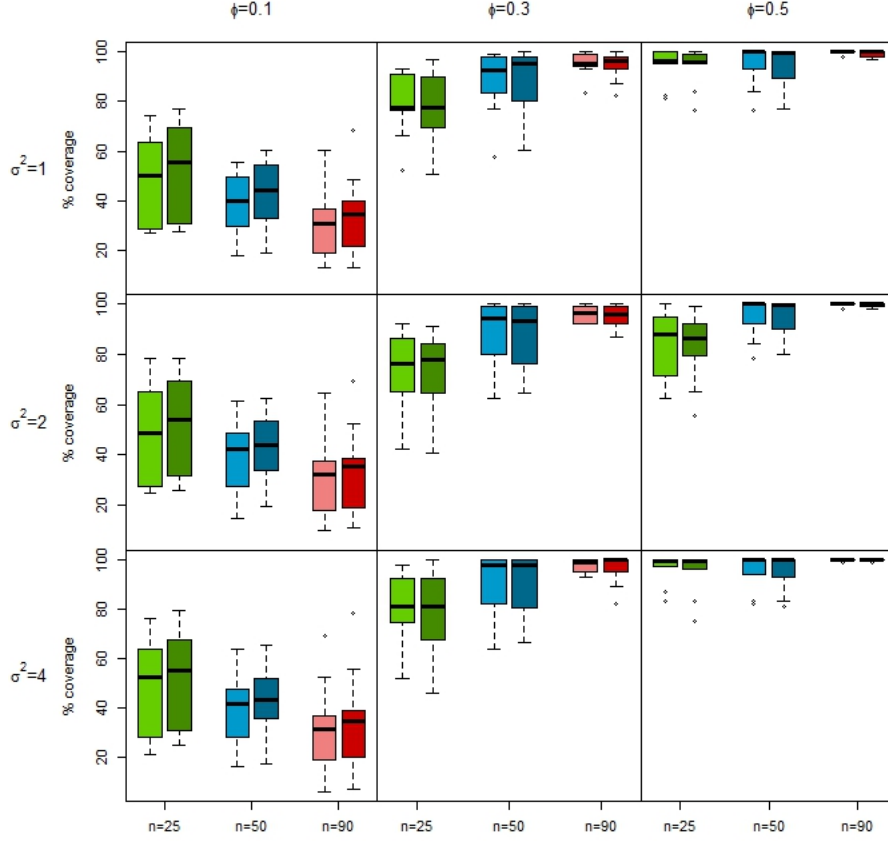


Figure 7: Boxplot of prediction band coverage for $n=25$, 50 and 90 and all 9 simulation scenarios. Lighter colours correspond to depth while darker colours correspond to distance as curves ordering criterion.

5 Real data analysis

5.1 Canadian temperature data

As first case study, we have chosen the well known data set of Canadian temperature data. This has been repeatedly used in the functional data literature (see, for example, [18, 10, 21, 25]). The data set consists of daily annual mean temperature collected at 35 meteorological stations in Canada's Maritimes Provinces: Nova Scotia, New Brunswick and Prince Edward Island, over the period 1960 to 1994. Note that the data set used here, which is the same as in [18, 10] covers a smaller geographical area than that in [21]. While other papers have been devoted to prediction of these temperature curves, our objective is to provide uncertainty bands for the predicted curves, and hence discussing the fitted model is out of the scope of this paper. To this aim, we have selected five stations at random to use as validation stations for which we will provide prediction

bands according to our proposal in Section 3. These can be seen in red in Figure 8 (left). Data were converted to functional observations through smoothing by using penalized cubic B-splines with 120 basis functions and penalty parameter equal to zero. These values were chosen using functional cross-validation. The FKED model, with longitude and latitude as covariates, was then fitted to the remaining 30 stations and predicted temperature curves were obtained (using ordinary functional kriging with an exponential variogram model) for the 5 validation stations. From the empirical trace-variogram, there was no evidence of a discontinuity at the origin and hence we fixed the nugget equal to zero. For each of the validation sites, a bootstrap sample of predicted curves of size $B = 1000$ was obtained using the smoothing parameter $\kappa = 0.05$. Band depth was calculated using the modified version *MBD*. The resulting 95% prediction bands are shown in Figure 9. The uncertainty bands are fairly narrow, as expected when observing the small variability between curves in Figure 8 (right). Overall, the two uncertainty measures seem to agree well, although in some cases the distance based prediction band appears to be slightly narrower than the depth based one. The bands appear to be wider for Station 1 than for the remaining stations, specially in winter, suggesting greater uncertainty in that station. This may be due to the fact that this is an inland station, while the other four validation stations are closer to the coast.

Coverage percentages of the original data for all 5 validation sites are summarized in Table 1. The coverage seems good, ranging from 71.2 to 95.1, when excluding the site 24 that has a lower coverage although it is over 60%.

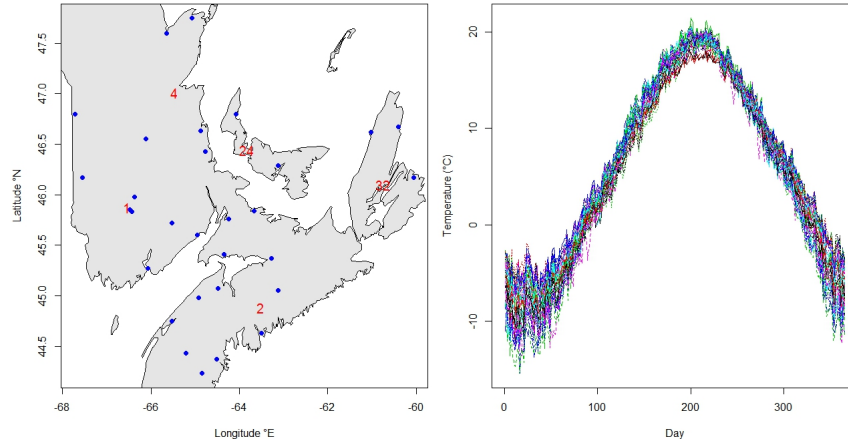


Figure 8: Left figure: locations of the 35 meteorological stations in Canada’s Maritimes Provinces area (validation stations numbered in red). Right figure: temperature curves (raw data)

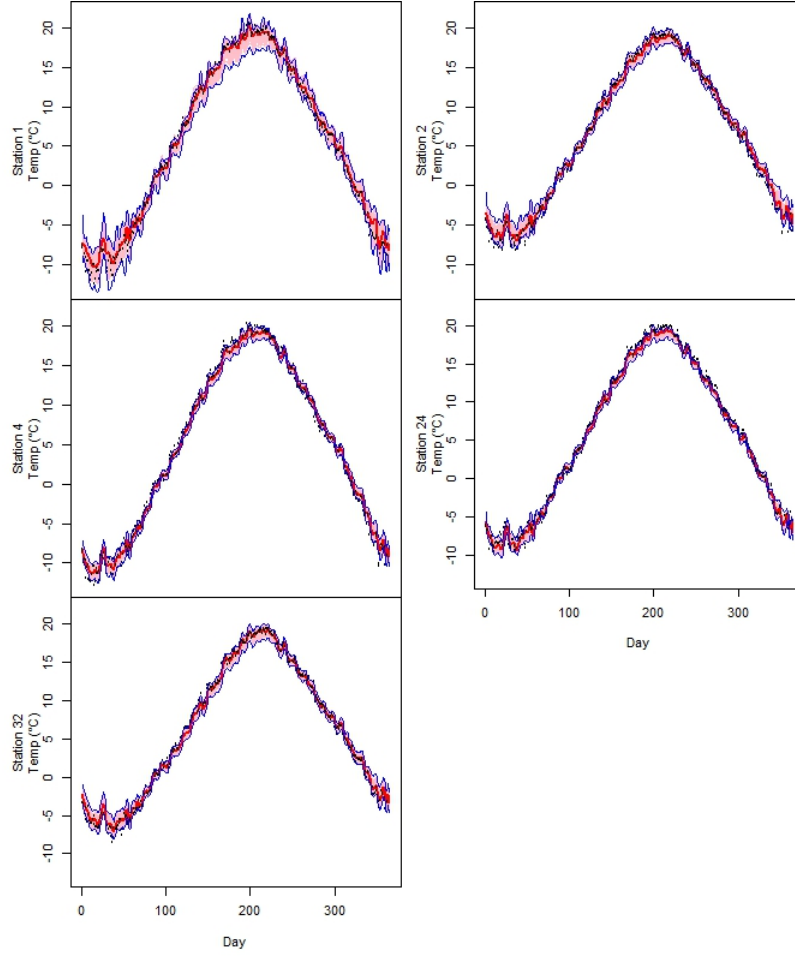


Figure 9: Original temperature data (black dots), FKED predicted curve (red line), 95% prediction ball (pink) based on L^2 distance and 95% prediction band (blue line) based on MBD for validation stations

Validation site	% coverage	
	distance	depth
1	94.8	95.1
2	81.9	83.3
4	71.2	75.3
24	62.7	66.0
32	89.3	89.9

Table 1: Percentage coverage for the 5 Canadian validation sites with $\kappa = 0.05$.

5.2 Air pollution data

The second case study considered consists of daily PM_{10} concentrations (in $\mu g/m^3$) measured in 24 sites (red triangles in Figure 10) from October 2005 to March 2006 by the monitoring network

of Piemonte region (Italy). Measurements were also available at 10 additional locations (blue dots in Figure 10) that are used as validation stations. Apart from geographical information, i.e. longitude, latitude and altitude of each station, considered as scalar covariates, information was available on daily maximum mixing height, daily total precipitation, daily mean wind speed, daily mean temperature and daily emission rates of primary aerosols, taken as functional covariates. These are available thanks to a nested system of deterministic computer-based models implemented by the environmental agency ARPA Piemonte [7]. This data set had already been analyzed in Cameletti et al. [2]. For further details on the model the reader is referred to Ignaccolo et al. [15]. A log transformation was used on the response variable to achieve normality and stabilize within-station variability. Prior to modelling, data (both response and functional covariates) were smoothed by means of cubic B-splines with 146 basis functions and penalty parameter equal to 0. These values were chosen using functional cross-validation [15].

The functional kriging with external drift model described in Section 2 was applied to the air pollution data, including the (standardized) scalar and functional covariates mentioned above, to obtain prediction curves (via ordinary kriging for functional data with an exponential variogram model and zero nugget) at the 10 validation sites. To obtain 95% prediction bands for each of the predicted curves, a bootstrap sample of size 1000 was obtained for each site following the algorithm proposed in Section 3. The effect of the smoothing parameter κ in this case was negligible. The results shown here are for $\kappa = 0.005$. We obtained prediction bands according to both the band depth and distance induced order. Band depth was calculated using the modified version *MBD* with $k = 2$. Prediction bands for the ten validation sites are shown in Figures 11 and 12, whereas coverage percentages of the original data are summarized in Table 2.

Validation site	% coverage	
	distance	depth
25 - Biella-Largo Lamarmora	94.5	94.5
26 - Borgo San Dalmazzo	94.5	95.1
27 - Bra	97.3	98.4
28 - Chivasso - Edipower	98.4	97.3
29 - Ivrea	84.1	80.2
30 - Saliceto	79.7	80.8
31 - Serravalle.Scrivina	94.5	95.1
32 - Susa	90.1	89.6
33 - Torino - Piazza Rivoli	99.5	99.5
34 - Torino - Via Gaidano	99.5	99.5

Table 2: Percentage coverage for the 10 validation sites in Piemonte with $\kappa = 0.005$.

Overall, the two uncertainty measures seem to agree well, although in some cases the depth based band appears to be slightly wider than the distance based one. The percentage of original

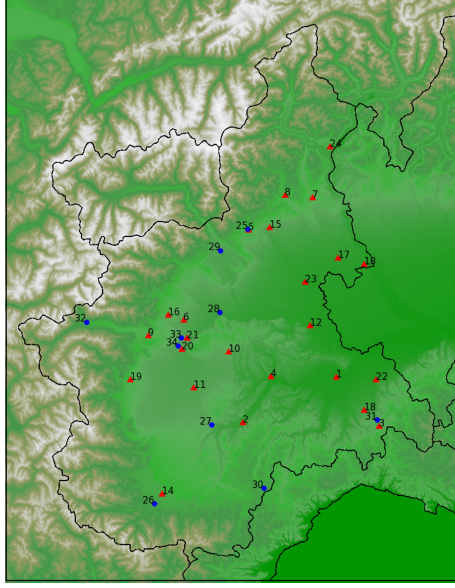


Figure 10: Locations of the 24 PM_{10} monitoring sites (red triangles) and 10 validation stations (blue dots).

data points contained in the prediction band varies from 79.7% (*Saliceto*) to 99.5% (*Torino - Via Gaidano*). This is in agreement with the predictions obtained from the FKED model, where the model performed fairly well in the latter validation site but poorly in the first.

6 Discussion

Measurements gathered over time at different spatial locations have been traditionally modelled from a spatio-temporal perspective. However, the domain does not necessarily need to be time, but it can be e.g. depth or height, giving rise to spatially dependent functional data. The functional kriging with external drift model allows to predict a whole curve - regardless the domain of the functional observations - taking into account exogenous covariates. The spatial correlation is accounted for when estimating the drift by means of an iterative algorithm. Nevertheless, uncertainty evaluation in the kriging context has not been addressed so far. In this paper, a semi-parametric bootstrap approach is extended to the functional case of spatially correlated data. The classic functional kriging variance provides a unique value over the whole domain T , while our aim is to provide an uncertainty measure whose value may change along the predicted curve. The proposed technique provides us with uncertainty bands around the predicted curve and, further, half the width of the resulting prediction band could be considered as an approximate margin of error.

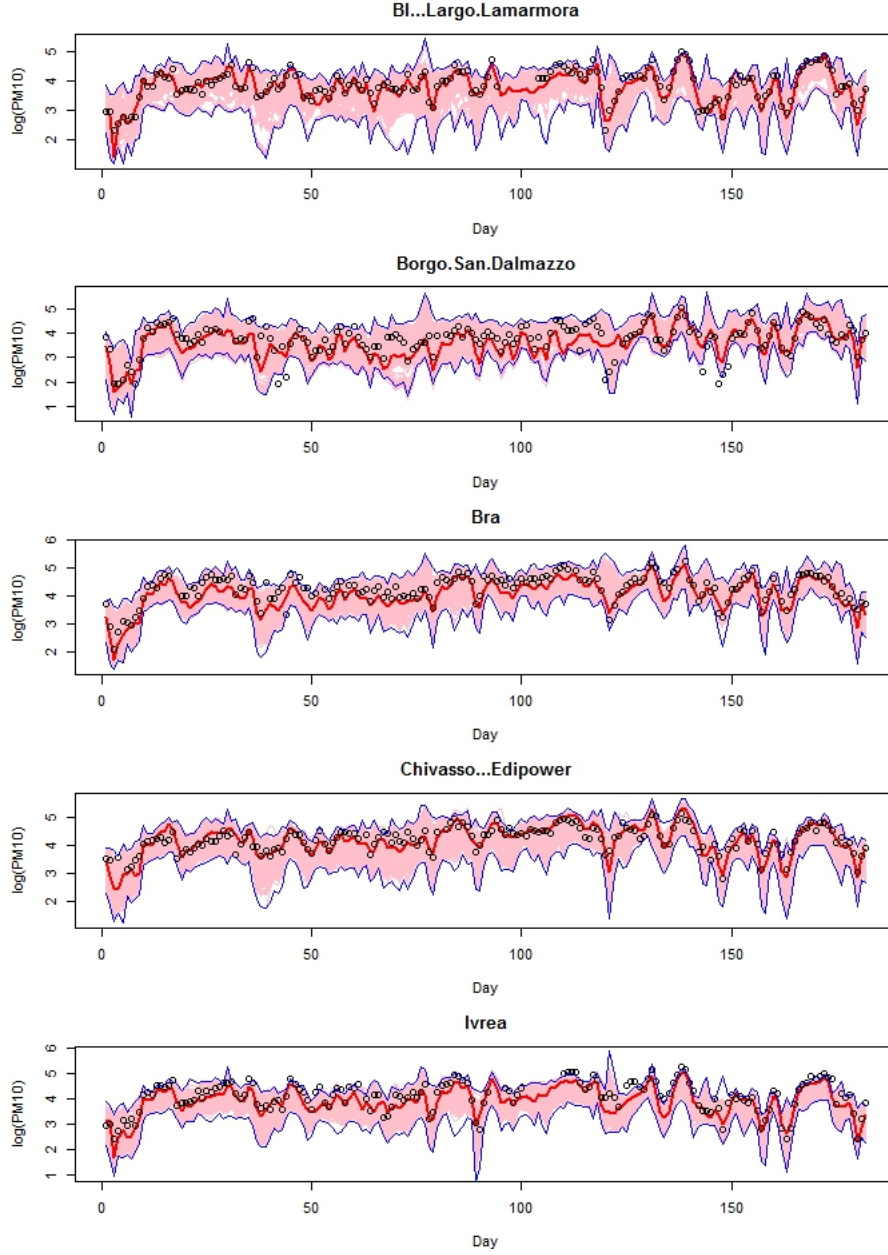


Figure 11: Original PM_{10} data (black dots), FKED predicted curve (red line), 95% prediction ball (pink) based on L^2 distance and 95% prediction band (blue line) based on MBD for validation stations (I).

The lack of an analytic expression of the kriging variance for a curve led us to use a bootstrap approach that not only allows the uncertainty to change over the domain T but also takes into account the uncertainty due to drift estimation. The bootstrap samples are obtained from a smoothed version of the empirical distribution function for which the smoothing parameter κ needs to be chosen in advance. On the other hand, a criterion to order the bootstrapped curves

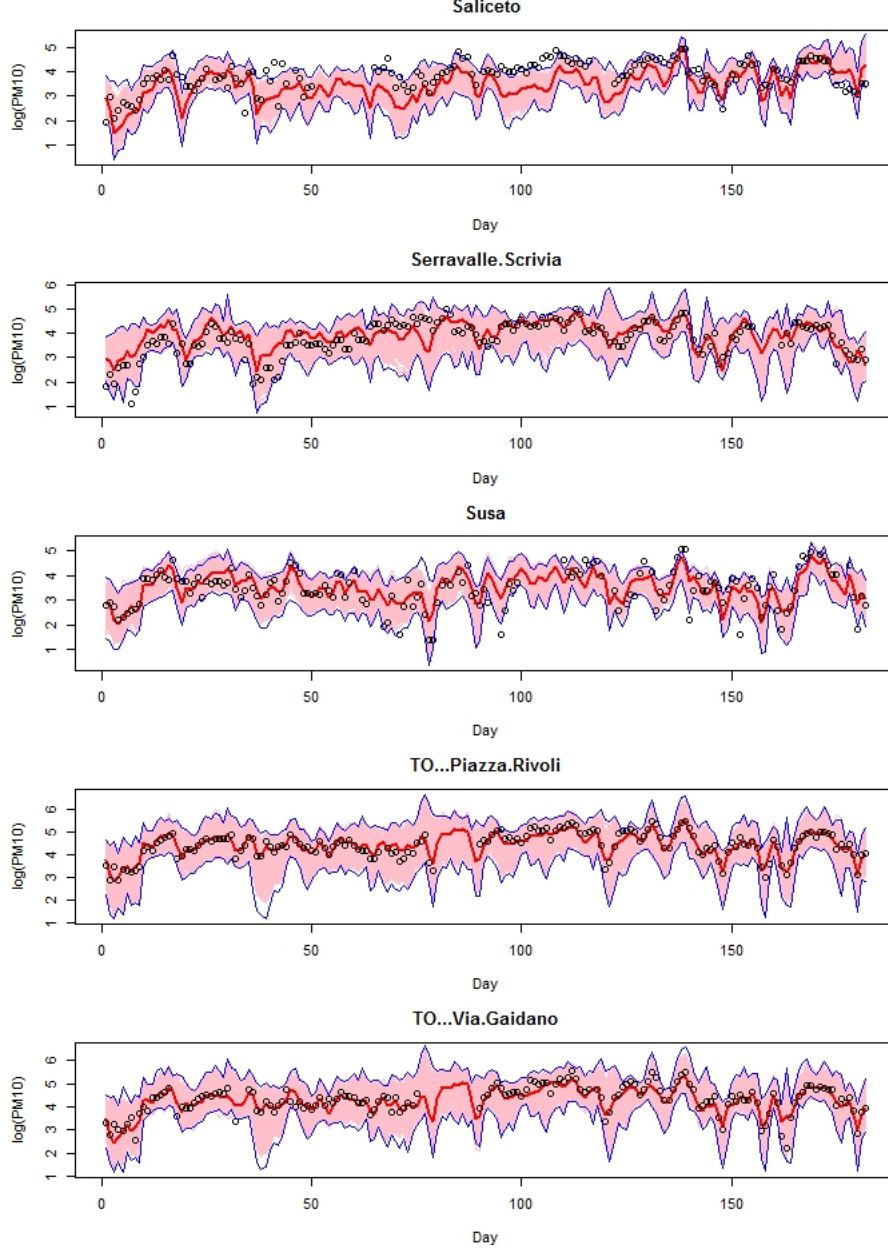


Figure 12: Original PM_{10} data (black dots), FKED predicted curve (red line), 95% prediction ball (pink) based on L^2 distance and 95% prediction band (blue line) based on MBD for validation stations (II).

needs to be adopted and we consider two different techniques proposed in the literature, namely functional depth and L^2 distance. To investigate the performance of the bootstrap approach as well as the effect of these choices, we set a simulation study where different values for spatial covariance parameters and sample size are considered. Moreover we apply the proposed technique to two real cases and illustrate the findings.

As for the two different ordering criteria, there is no great difference in the results for both the simulations and the two case studies. To be conservative, one could argue that it is safer to use the depth as this results in larger uncertainty since the depth criterion gives larger bands when the sample size is not so large.

Regarding the choice of κ , in the lack of previous indications, we tried some values in the different scenarios. Theoretically, as κ increases a larger artificial noise is added to the original data and hence curves present more variability, resulting in wider prediction bands and higher coverage, but this does not necessarily mean an improvement in the uncertainty evaluation. In practice, when there are not validation sites, a rule of thumb would be useful and this remains an open issue.

Overall, using the known data at validation sites in both simulations and real case studies, it can be concluded that the proposed method appears to be a valid approach in evaluating uncertainty for a predicted curve. In particular, the simulation study shows that the width of the bands depends on the scale and range of the covariance structure, at least for the exponential case, and becomes more stable over the domain T with increasing sample size.

In a previous work [8] for the PM₁₀ case study, functional principal component analysis (FPCA) was applied to the residual curves; in this case the resampling was carried out on the the scalar loadings of the PCA decomposition. The resulting prediction intervals were not very different but the approach does not involve bootstrap for functional data. As a further alternative, with a longitudinal point of view, we also considered a generalized additive model (GAM) with a smooth function of longitude, latitude and time, to predict a curve so that standard inference results apply. In the considered case study, FKED prediction outperformed GAM prediction even though with a larger uncertainty; nevertheless, the prediction interval provided by the GAM model is pointwise (and it could be corrected by the Bonferroni method) while our approach gives a simultaneous prediction band w.r.t. T .

Data in the two case studies considered in this paper were regularly spaced over the domain T ; however, that is not always the case (see e.g. atmospheric profiles in [14]). For irregularly spaced data, curves could be aligned at the initial smoothing step before fitting the functional kriging with external drift model, as it is straightforward to evaluate the curves for every $t \in T$ in a common grid for all curves.

The algorithm proposed for uncertainty evaluation of spatially correlated curves is computationally feasible and applies to a wide range of practical situations, as it can be used regardless of the complexity of the drift term, or even in the absence of the latter. Our proposal has been specified in the case of ordinary kriging where the weight coefficients are constant and the spatial structure is determined by means of the trace-variogram. However it may be the case that a more complex kriging alternative is desirable in order to let the weights vary with t (for both the real

data and the bootstrap samples). To be consistent with the way the kriging weights have been specified in the cases of continuous time-varying kriging and functional kriging total model, the underlying spatial structure (and hence the matrices K in Section 2 and Σ in Section 3) should not be determined by means of the trace-variogram. In fact, in [11] and [9] functional data are expressed as linear combinations of splines and a Linear Model of Coregionalization is used to estimate cross-correlations among the spline coefficients; this way a possible interaction between the curve domain and the space domain is taken into account. Consequently the matrices K and Σ could be adjusted accordingly but with the added burden of an increased computational load.

We believe that the method proposed in this paper is appropriate in the framework of functional data and is able to provide uncertainty bands for a predicted curve in an unmonitored site. We think this will prove useful for monitoring purposes and policy assessment where the uncertainty should always accompany the related prediction.

7 Acknowledgments

This work was supported by “Futuro in Ricerca” 2012 Grant (project no. RBFR12URQJ, named StEPHI) provided by the Italian Ministry of Education, Universities and Research. The authors are grateful to Alan Gelfand and all the participants of the StEPHI intermediate workshop for the fruitful discussion.

References

- [1] W. Caballero, R. Giraldo, and J. Mateu. A universal kriging approach for spatial functional data. *Stochastic Environmental Research and Risk Assessment*, 27(7):1553–1563, 2013.
- [2] M. Cameletti, R. Ignaccolo, and S. Bande. Comparing spatio-temporal models for particulate matter in piemonte. *Environmetrics*, 22(8):985–996, 2011.
- [3] J.-P. Chiles and P. Delfiner. *Geostatistics: Modeling Spatial Uncertainty, 2nd Edition*. Wiley, Hoboken, NJ, 2012.
- [4] A. Cuevas, M. Febrero, and R. Fraiman. On the use of the bootstrap for estimating functions with functional data. *Computational Statistics and Data Analysis*, 51:1063–1074, 2006.
- [5] P. Delicado, R. Giraldo, C. Comas, and J. Mateu. Statistics for spatial functional data: some recent contributions. *Environmetrics*, 21:224–239, 2010.

- [6] F. Ferraty, I. Van Keilegom, and P. Vieu. On the validity of the bootstrap in non-parametric functional regression. *Scandinavian Journal of Statistics*, 37:286–306, 2010.
- [7] S. Finardi, R. De Maria, A. D’Allura, C. Cascone, G. Calori, and F. Lollobrigida. A deterministic air quality forecasting system for Torino urban area, Italy. *Environmental Modelling and Software*, 23(3):344–355, 2008.
- [8] M. Franco-Villoria and R. Ignaccolo. Kriging uncertainty for functional data: a comparison study. In *Proceedings of the METMAVII–GRASPA 14 Conference. Special issue of GRASPA Working Paper*, 2014.
- [9] R. Giraldo, P. Delicado, and J. Mateu. Geostatistics with infinite dimensional data: a generalization of cokriging and multivariable spatial prediction. Technical report, Reporte Interno de Investigacion No. 14, Universidad Nacional de Colombia, 2009.
- [10] R. Giraldo, P. Delicado, and J. Mateu. Continuous time-varying kriging for spatial prediction of functional data: an environmental application. *Journal of Agricultural, Biological, and Environmental Statistics*, 15(1):66–82, 2010.
- [11] R. Giraldo, P. Delicado, and J. Mateu. Ordinary kriging for function-valued spatial data. *Environmental and Ecological Statistics*, 18(3):411–426, 2011.
- [12] M. Goulard and M. Voltz. Geostatistical interpolation of curves: A case study in soil science. In A. Soares, editor, *Geostatistics Troia 92*, pages 805–816. Kluwer Academic, Dordrecht, 1993.
- [13] L. Horváth and P. Kokoszka. *Inference for functional data with applications*. Springer, New York, 2012.
- [14] R. Ignaccolo, M. Franco-Villoria, and A. Fassò. Modelling collocation uncertainty of 3D atmospheric profiles. *Stochastic Environmental Research and Risk Assessment*, 29(2):417–429, 2015.
- [15] R. Ignaccolo, J. Mateu, and R. Giraldo. Kriging with external drift for functional data for air quality monitoring. *Stochastic Environmental Research and Risk Assessment*, 28:1171–1186, 2014.
- [16] N. Iranpanah, M. Mohammadzadeh, and C.C. Taylor. A comparison of block and semi-parametric bootstrap methods for variance estimation in spatial statistics. *Computational Statistics and Data Analysis*, 55:578–587, 2011.

- [17] S. Lopez-Pintado and J. Romo. On the concept of depth for functional data. *Journal of the American Statistical Association*, 104(486):718–734, 2009.
- [18] A. Menafoglio, P. Secchi, and M. Dalla Rosa. A universal kriging predictor for spatially dependent functional data of a Hilbert space. *Electronic Journal of Statistics*, 7:2209–2240, 2013.
- [19] D. Nerini, P. Monestiez, and C. Manté. Cokriging for spatial functional data. *Journal of Multivariate Analysis*, 101:409–418, 2010.
- [20] R Core Team. *R: A Language and Environment for Statistical Computing*. R Foundation for Statistical Computing, Vienna, Austria, 2015.
- [21] J. Ramsay and B.W. Silverman. *Functional Data Analysis*. Springer, New York, 2006.
- [22] J. O. Ramsay, Hadley Wickham, Spencer Graves, and Giles Hooker. *fda: Functional Data Analysis (R package version 2.4.4)*.
- [23] A. Reyes, R. Giraldo, and J. Mateu. Residual kriging for functional spatial prediction of salinity curves. *Communications in Statistics - Theory and Methods*, 44(4):798–809, 2015.
- [24] G.K. Robinson. That BLUP is a good thing: the estimation of random effects. *Statistical Science*, 6:15–32, 1991.
- [25] F. Scheipl, A.M. Staicu, and S. Greven. Functional additive mixed models. *Journal of Computational and Graphical Statistics*, 2014.
- [26] T. Speed. Comment on paper by Robinson. *Statistical Science*, 6:421744, 1991.
- [27] Y. Sun and M. Genton. Functional boxplots. *Journal of Computational and Graphical Statistics*, 20(2):316–334, 2011.
- [28] Y. Sun, M. Genton, and D.W. Nychka. Exact fast computation of band depth for large functional datasets: How quickly can one million curves be ranked? *Stat*, 1:68–74, 2012.
- [29] S.N. Wood. *mgcv: Mixed GAM Computation Vehicle with GCV/AIC/REML Smoothness Estimation (R package version 1.8.6)*.
- [30] S.N. Wood. *Generalized Additive Models: An Introduction with R*. Chapman and Hall/CRC, 2006.
- [31] S.N. Wood. Fast stable restricted maximum likelihood and marginal likelihood estimation of semiparametric generalized linear models. *Journal of the Royal Statistical Society (B)*, 73(1):3–36, 2011.